J Nanostruct 15(2): 652-665, Spring 2025

RESEARCH PAPER

Synthesis and Characterization of γ-Alumina Porous Granules by Aluminium Nitrate Precursor as an Efficient Catalyst Support

Hamideh Rafipoor [1], ***Seyed Mohammad Mirkazemi*** [1]*, ***Yaser Vahidshad*** [2], ***Zahra Amirsardari*** [2]

[1] *School of Metallurgy and Materials Engineering, Iran University of Science & Technology (IUST), Narmak, Tehran, Iran*

[2] *Space Transportation Research Institute, Iranian Space Research Center, Tehran, Iran*

ARTICLE INFO

Article History:
Received 07 January 2025
Accepted 25 March 2025
Published 01 April 2025

Keywords:
Catalyst support
Oil-drop
Sol gel, Iridium
γ- alumina granules

ABSTRACT

Gamma-alumina (γ-Al_2O_3) granules were synthesized as iridium catalyst supports for hydrazine decomposition. The granules have new physical and textural properties which are critical in determining the catalytic performance. Aluminium nitrate precursor changes the structure of γ-Al_2O_3 and affects the support interactions at 450 °C and 750 °C. This leads to the facile gas exhaust and makes it more resistant to the pores of the catalyst during decomposition of hydrazine monohydrate. As a result, higher conversion of hydrazine and selectivity to hydrogen is achieved compared to the catalysts prepared by supports that are crushed. The γ-Al_2O_3 granules with mechanical strength from 7.12 to 25.56 N/granule is obtained. Specific surface area, volume and the diameter of porous granules are 346.02 m^2/g, 4.94 nm, 0.29 to 0.43 m^3/g, respectively.

How to cite this article
Rafipoor H., Mirkazemi S., Vahidshad Y., Amirsardari Z. Synthesis and Characterization of γ-Alumina Porous Granules by Aluminium Nitrate Precursor as an Efficient Catalyst Support. J Nanostruct, 2025; 15(2):652-665. DOI: 10.22052/JNS.2025.02.025

INTRODUCTION

Alumina is an important class of engineering material that is widely used in the various fields of industry, such as ceramics, metallurgy, and electronics because of its excellent electrical insulation, high corrosion resistance, and catalytic properties. Among metastable phases of alumina, γ-Al_2O_3 is usually used in adsorbents and catalysts [1]. The catalyst support based on alumina sources is usually used in manufacturing catalytic systems such as pyrolysis, gasification, chemical looping combustion and other thermo-catalytic conversion methods [2-6]. This variety of uses are due to its unique features like high surface area, acidity, and mesoporous structure [7, 8]. In fixed bed reactors, spherical granules give a uniform catalyst bed efficient for reducing pressure drop on them [9, 10]. In general, improvement of catalyst support properties such as structure and type of material composition, typically results in remarkably improved catalyst activity [11]. The spherical granules have problems such as weak mechanical resistance, low attrition resistance, and randomly granule size distribution [12]. Therefore, it is important to synthesis a stable support to improve catalytic performance of the catalyst without mass loss and crushing parts during decomposition of fuel. Various precursors can be used for gamma-alumina preparation, but the development of efficient support for gas generation with high

---

* *Corresponding Author Email: mirkazemi@iust.ac.ir*

catalyst activity in the hydrazine decomposition process is critical importance. One of the major challenges in the decomposition process is the mass loss of supports, and these defects make the granules unusable in the reactors [13, 14]. Therefore, the synthetic optimization of support is required for the proper operation of the bed. In the earlier decades, γ-alumina has been manufactured by any traditional paths such as precipitation [15, 16], combustion [17], hydrothermal [18, 19], sol-gel [20, 21], and mechanical synthesis [22]. The sol-gel method is a suitable technique for the synthesis of catalytic supports. The starting materials employed for the sol-gel method can be different reagents such as metallic salts, metallic oxides, metallic hydroxides, metallic complexes, or metal alkoxides. They should be soluble in the reaction medium and reactive sufficient to aid in the gel-forming process. The sol-gel presses is divided into the subsequent steps: solution formation, gelation, aging, drying, and densification by ending heat treatments [23]. Surface atoms mainly form nanomaterials, which decreases particle size. This leads to an increase in the ratio of surface area to volume of granules [24].

The received granules via this route have an equal granule size, exceptional mechanical properties, and adjusted pore size distribution [25]. In sol-gel method alumina hydrosol formation is the first level [26]. Depending on the congealing, the liquid phase molding has divided into two distinct paths: hydrocarbon-ammonia and oil-drop methods [27]. The hydrocarbon-ammonia route is more costly than the oil-drop process due to use of aluminium lakeside or pseudo-boehmite as boehmite precursor. The oil-drop technique is a promising route to develop γ-alumina spheres [28].

In the present study for the first time we reported that the γ-Al_2O_3 supporting iridium granules exhibited excellent performance in the hydrazine decomposition that was synthesized by aluminium nitrate precursor through the oil-drop method. The study examines all parameters affecting the synthesis conditions on γ-Al_2O_3 such as sol with different molarities, aging times, sedimentation methods, precipitating agents, calcination temperatures, different concentrations of acid and base, an effective approach for maintaining the catalytic performance of Ir@γ-Al_2O_3. The aim is to find a stable support and introduce it to the active catalyst. The synthesized alumina granules were characterized by TGA/DTA, XRD, OM, BET and crush strength.

MATERIALS AND METHODS

All chemicals were of analytical grade and purchased from Merck without further

Table 1. Details of synthesized for preparation of γ-alumina granules.

Sample No.	Synthesis Solution			Aging time in oil column (h)
	HNO_3 (M)	H/Al (mol/mol)	OH/Al (mol/mol)	
1NS	1.00	0.011	1.734	2.0
2NS	1.00	0.023	2.028	1.5
3NS	1.00	0.026	3.133	0.0
4NS	3.00	0.030	2.550	-
5NS	3.00	0.960	2.866	0.0
6NS	6.00	1.440	2.150	-
7NS	0.50	0.026	2.800	0.0
8NS	14.33	0.026	2.800	0.0
9NS	2.00	0.026	2.800	0.0
10NS	3.00	0.026	2.800	0.0
11NS	0.25	0.026	2.800	0.0
12NS	0.50	0.026	2.800	0.5

purification.

Gamma-alumina preparation

Aluminium nitrate ($Al(NO_3)_3.9H_2O$, 95%) solution 0.1 M was prepared. The starch solution (4%) was made at 60°C with a stirrer for 20 min and added to the initial solution at a weight ratio of 2.8% starch to aluminium nitrate. The mixture was stirred at high speed for 2 h to homogenize the solution at ambient temperature. After stirring, the resulting solution was transferred to a syringe pump with a rate of 1 ml/min under constant stirring until the pH of the solution reached about 8-9. After 24 h age at room temperature, the precipitate was separated by centrifugation (4000 rpm for 2 min) and washed several times with distilled water at pH=7. A certain amount of nitric e (HNO_3 with different molarity) was added to the sol under constant stirring and placed in a 50 Hz bath ultrasonic for 3 min. To increase the viscosity of the sol and turn it into a gel, the sample was heated to 70 ℃ under constant stirring and kept at this temperature for about 1- 2 h. The gelled sol was injected by a syringe pump at a rate of 1 ml/min into a column containing 10 % ammonia solution (NH_4OH 1M). Then the granules aged in the paraffin oil at 85 ℃ for 1 h (Table 1), and finally granules were washed several times with distilled water, then dried in an oven at 40 ℃ for 48 h. The dried granules calcined at 450 °C or 750 ℃ for 3 h at a heating rate of 2 ℃/min, then cooled down to room temperature at a rate of 5 °C/min. All samples were denoted as nNS-450 and nNs-750, which were calcined at 450 ℃ and 750 ℃, respectively.

Iridium@gamma-alumina catalyst preparation by porous impregnation

Synthesis of iridium catalysts was done by a wet impregnation method on the optimal support. The required amount of $H_2IrCl_6 \bullet H_2O$ was weighed and dissolved in deionized water at room temperature. The pH adjustment was controlled with small amounts of HCl. Then, a specified amount of support was added to the 20 wt% solution of iridium. The slurry was stirred at 60 ℃. After this step, the samples were kept at 80 ℃ in an oven for 12 h, and at 400 ℃ in a furnace under an air atmosphere for 3 h, and subsequently reduced in a tubular furnace under H_2 atmosphere at 400 ℃ for 2 h.

Characterization of the catalyst samples

X-ray diffraction Utilizing the Explore GNR with a copper cathode electron gun and a nickel filter to produce a single-phase beam k_α with a wavelength of 1.5 Å, and a detector with a step of 0.05 with a difference in potential of 40 kV and current intensity of 30 mA. The optical microscopy (OM) and scanning electron microscopy (SEM) images were taken by LICA MICROSYSTEMS and MIRA3 TESCAN, respectively. The specific surface area, diameter, and porosity of the samples were measured by BELSORP MINI II at 77 K. STA analysis was performed as weight analysis (TG) and thermal analysis (DTA) by PerkinElmer with an alumina pan at 10-1000 °C. To measure the resistance of the granules to compressive stress, according to the international standard Instron 4465 (Universal testing instrument), the samples were detected by inspecting 50 tables. The granule rested on the mandible, which was fixed, and the maxilla moved toward the mandible at a rate of 2 mm/min. The result of this experiment is the maximum force required to break the granule, reported as Newton on the granule (N⁄granule).

Catalytic performance testing

The measurement of catalytic decomposition of $N_2H_4 \cdot H_2O$ (hydrazine monohydrate) was conducted in a 100 ml four necked round-bottomed flask and stainless reactor. In a typical run, the flask containing 0.02 g catalyst was held at the room temperature, and then 10 ml $N_2H_4 \cdot H_2O$ was injected into the flask to initiate the decomposition reaction. The gaseous products (H_2, N_2, and NH_3) were allowed to pass through a trap containing 1.0 M HCl to absorb ammonia, and then evaluated by means of a gravimetric water-displacement method using an electronic balance every 500 ms. The reaction rate or TOF was evaluated at the hydrazine conversion of 80%. The hydrogen selectivity (X), and TOF were determined by Eq. 1 [29].

$$X=\frac{3\frac{n(N_2)+n(H_2)}{n(N_2H_4)}-1}{8} \qquad (1)$$

$$TOF=\frac{PV}{3n_{metal}RTt} \qquad (2)$$

$$\mathrm{Al(NO_3)_3 + 3NH_4OH \rightarrow Al(OH)_3 + 3NH_4NO_3} \tag{3}$$

$$\mathrm{Al(OH)_3 \rightarrow AlOOH + H_2O} \tag{4}$$

$$\mathrm{13Al(OH)_3 + 7H^+ + H_2O \rightarrow [\,AlO_4Al_{12}(OH)_{24}(OH_2)_{12}]^{7+}} \tag{5}$$

Where, the universal gas constant is R, the reaction temperature is T, the atmospheric pressure is P, the mole number of iridium is n_{Ir}, the volume of H_2 and N_2 is V, and the reaction time is t.

RESULTS AND DISCUSSION

By mixing the aluminium nitrate in water and the ammonia solution according to the reaction (3), aluminium hydroxide precipitate is formed.

As the aging time progresses, according to the reaction (4) the aluminium hydroxide precipitate becomes boehmite.

Both amorphous aluminium hydroxide and boehmite are stable in an alkaline solution, but the amorphous aluminium hydroxide dissolves easily in an acidic solution. Therefore, the use of acid has been for both purposes of peptize and removal of aluminium hydroxide. Aluminium hydroxide reacts with acid according to the reaction (5) to form the Al^+ polymer chains.

And the other part of the acid does the peptize operation to have smaller particles of boehmite in the sediment. These two phenomena occur simultaneously.

In this study, the different molarities of nitric acid (0.25, 0.5, 2, 3, and 14.33) were used by keeping the [H] and [OH] to [Al] ratios constant at 0.026 and 2.8 in the 7NS to 11NS samples, respectively. The value of higher molarities leads to a higher viscous gel that is not suitable for production of droplets. The sol with 0.5 M nitric acid produced an excellent gel with a suitable viscosity to produce granules by the oil drop method. The viscosity of the gel should be such that it produces droplets with enough strength to maintain their shape during the process of forming and washing.

The properties of the resulting gel show a higher sensitivity to the [H]-to-[Al] ratio than to the sol acidity, so it is better to use the [H]-to-[Al] ratio in the sol as a variable factor instead of acidity. By preparing sol samples with different [H] to [Al] ratios that lead to a definite acidity from 0.011 to 1.44 (1NS to 7NS samples); it is observed that only sol with [H]-to-[Al] ratio 0.026 had good quality and produced a homogeneous gel. If higher or lower molarity of [H]-to-[Al] ratio is used, only the sol becomes more concentrated and a high viscosity gel is obtained, which is not suitable for dropping and spherical granule formation. On the other hand, instead of acidity, the ratio of [OH]-to-[Al] has been changed. Ammonia solutions (1M) and have been employed to precipitate the sol. no suitable gel was obtained in samples 1NS to 7NS sols prepared with a certain acidity (pH=8-9) and various ratios of the [OH]-to-[Al] from 1.7 to 3.13. The gels with the [OH]-to-[Al] ratio higher than 2.8 did not dissolve after washing, but the gel with the [OH]-to-[Al] ratio of 2.8, in addition to not dissolve after aging and washing, had the desired quality and shape of granules. Therefore, it was selected as the optimum ratio. The adsorbed layer around each particle, like a barrier, prevents the particles from coming together and coagulation. Unlike electrostatic stability, there is no repulsive force and when the molecules come in contact with each other, the particles are exposed to gravitational forces. In other words, some long polymer chains absorb several particles on their surface. For this purpose, due to the chain nature of starch, the starch has been used as a space barrier. The calcination of the samples was occurred at 450 °C and 750 °C, by placing the gel granules in the ammonia solution, the crosslinks in the gel network become wider and the compaction step occurs.

After dropping gel, in some samples, some droplets of gel accumulated at the layer between ammonia and oil and formed into clusters. To solve this problem, the granules were first dropped into the oil column and after aging; they were added in ammonia solution and remained for one hour. Examining the 0.5, 1.5, 2 h for aging terms in the oil showed that minimum time (0.5 h) is suitable for this purpose. In fact, a thin layer of oil covered the granule particles and prevented them from sticking together in ammonia during this time. facial features the granules are listed in the Table 2.

Morphological characterization by OM and SEM

The images of the granules taken by optical photograph are shown in Fig. 1. The sample 3NS-450 has a high ratio of [OH]-to-[Al] which leads to the presence of ammonia or additional compounds in the gel and most granules are destroyed during the washing step, as shown in Fig. 1(a). The sample 5NS before calcination has a high ratio of [H]-to-[Al], which causes a lot of bubbles in the gel and the wet granules were not sufficiently strong to retain spherical shape so the non-uniform size and sphericity of granules were obtained (Fig. 1 (b)).

The desired gel from the perspectivie of viscosity and strength (sample 7NS-450) with appropriate ratios of [H]-to-[Al] and [OH]-to-[Al] is obtained which resulted in good granules produced as the sphericity and appearance. The only problem with this sample was the collection of gel droplets at the oil-ammonia interface. To solve this problem, the drops fell into the ammonia by hand moving, causing the granules to become irregular (Fig. 1(c)).

By keeping the constant ratio of [H] or [OH] to [Al] and increasing the molarity of the acid (0.026 and 2.8 respectively) yet high concentrations of acid (above 2M) have been used in their production. It was observed that the viscosity of the gel increased which resulted in irregular or cylindrical granules, as shown in Fig. 2a-d. The lowest molarity of acid (0.25 M) in sample 11NS-450 leads to accumulate of the droplets at the interface between the oil and ammonia, clumping together and forming clusters (Fig. 2e).

The optical images of the sample 12NS at different calcination temperatures are shown in the Fig. 3. In this sample, by using 0.5M acid the molar ratio of [H] and [OH] to aluminium was appropriate (0.026 and 2.8, respectively). The viscosity of the gel obtained from this sample was suitable for droplets, which finally resulted in the production of spherical and regular droplets. The gel sample 12NS has the same conditions as the gel sample 7NS, except that it has three times the volume and has good reproducibility. To avoid the accumulation of gel droplets at the interface of ammonia and oil in the sample 12NS-450 and 12NS-750, the droplets were first poured into oil for 30 min, and poured into the ammonia solution. Finally, regular spheres were obtained by this process. The average diameter of the sample granules 12NS before calcination, 12NS-450, and 12NS-750 are 1.75, 1.71, and 1.64 mm, respectively.

Fig. 4 shows the morphology of the surface and cross section of 12NS-450 and 12NS-750 granular. The produced granules are sphere shape and homogenous with the small hairline cracks was observed on the surface of 12NS-450 and 12NS-750 granular which may create in the drying or calcination step. The pores on the surface of the granules of the 12NS-450 sample are visible, with

Table 2. Facial features of granules.

Sample No.	1NS	2NS	3NS	4NS	5NS	6NS
Condition of granules after washing	solved	solved	Crushed	solved	Crushed	pseudo spherical
	7NS	8NS	9NS	10NS	11NS	12NS
	pseudo spherical	pseudo spherical	pseudo spherical	pseudo spherical	cluster	spherical

Fig. 1. Optical photograph of (a) 3NS-450, (b) 5NS-450, and (c) 7NS-450 granular samples.

increasing calcination temperature the pores on the surface of the granular are reduced by sintering. At higher magnifications [13], a large number of porosities due to the amorphous nature of γ-alumina are observed with uniformly distributed cavities. According to FE-SEM images, the granules have interparticle porosity and their internal connections have led to the formation of channels. Due to the presence of these channels, the shape and size of the pores are not recognizable. As the calcination temperature of the granules increases, the surface roughness increases. It is considered that the morphology of the particles in the granules calcinated at 750 ℃ is more agglomerated as compared with granular calcinated at 450 ℃.

Surface area analysis

The pore structure of the alumina depends greatly on the conditions of the heat-treatment [30]. Fig. 5 shows the nitrogen adsorption-desorption isotherm of sample calcined at two temperatures with the mesoporous structures and type IV isotherms (IUPAC classification) that reveals the interconnectivity of pores [31]. The type IV isotherm is a suggestion of the monolayer adsorption observed by multilayer formation and capillary condensation [32]. The interconnectivity of the pores was revealed by a sharp step on desorption isotherm in Fig. 5a. When a channel is connected to the outside vapor phase within a smaller pore, this pore usually works as a neck (which is identified as ‘‘ink-bottle’’ pore) [30]. The isotherms for both of calcined granules are the combination of H_2 and H3-type hysteresis loops characteristic. In the H_2 type, the variation of slope in the two branches of adsorption and desorption represents the interconnectivity of the pores. This type of loop shows the presence of pores by a shape similar to a bottleneck, wedge-shaped, or parallel plates [33]. The main uptake observed at high relative pressures (P/P_0) expanse 0.28–0.98 for calcined granules at 450 ℃ and 0.3–0.98 for the calcined granules at 750 ℃. Adsorption in this range was due to the filling of mesopores [34]. Moreover, the hysteresis loop for the desorption process in a similar pressure range was further evidence that mesopores had been created. Both samples had a high specific surface area, and as the heat treatment temperature increased, the specific surface area decreased as the holes became larger and the porosity developed.

The hysteresis loop of the calcined sample at 750 °C occurred at higher relative pressures with larger pores. On the other hand, the hysteresis loop of the calcined sample at 450 °C indicates that the nitrogen used in this test is higher due to the specific surface area. The pore size distribution curves for microspheres calcined at different temperatures obtained from the Barrett–Joyner–

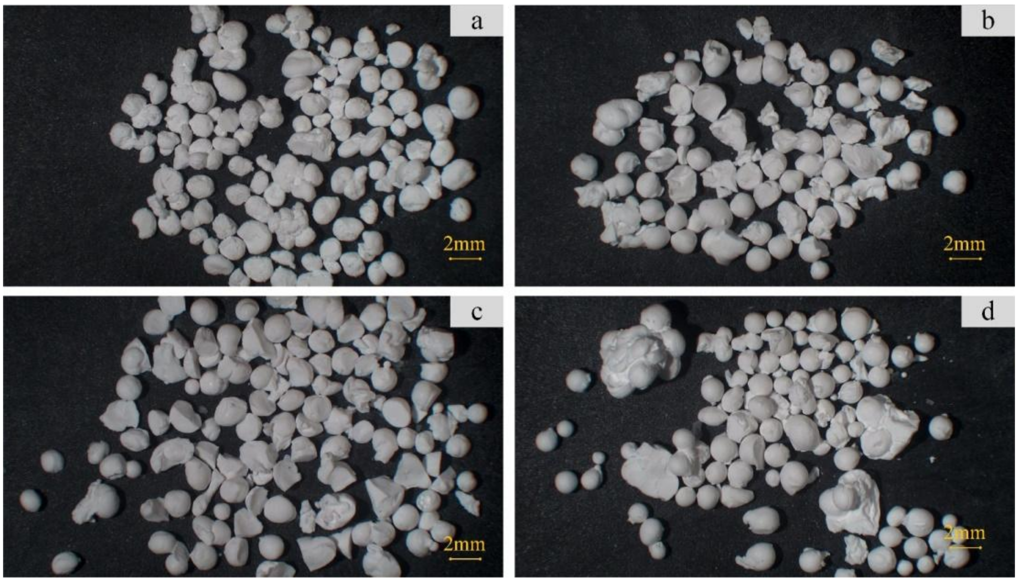

Fig. 2. Optical photograph of granular (a) 8NS-450, (b) 9NS-450, (c) 10NS-450, and (d) 11NS-450 samples.

Halenda (BJH) method is shown in Fig. 5b and Table 3. As calcination temperature increases, the specific surface area decreases, and the size of the pores increases [35]. However, the surface area of γ-alumina usually decreases at higher temperatures due to sintering and the phase transition to the α-alumina. We besides frustrated to compare the pore volume, pore diameter and BET surface area of catalyst support (granules) of our produced and other reported research Table 3.

Thermal gravimetric analysis

The DTA and TGA curves for the gamma-alumina granules of optimum sample are shown in Fig. 6. The TGA curve shows two steps of weight loss at various temperatures, the first step about 70 ℃ to 250 ℃ corresponds to outflow physically adsorbed water and breaking the chemical bonds of water with the surface of the boehmite. The sample suffered from a major weight loss in the temperature range of 250–350 ℃ due to the decomposition of both types of hydroxy groups present in boehmite, which includes external and internal groups between the layers of boehmite to form Al–O–Al oxy bridges. At about 300 °C, an exothermic peak is formed as the decomposition of amylose and amylopectin in starch. But then, at 320 °C, a great endothermic peak appeared to break the Al-O-Al and Al-OH bonds [41]. About 450 °C, the boehmite transferred to gamma-alumina. The wide endothermic pick arraying from 400

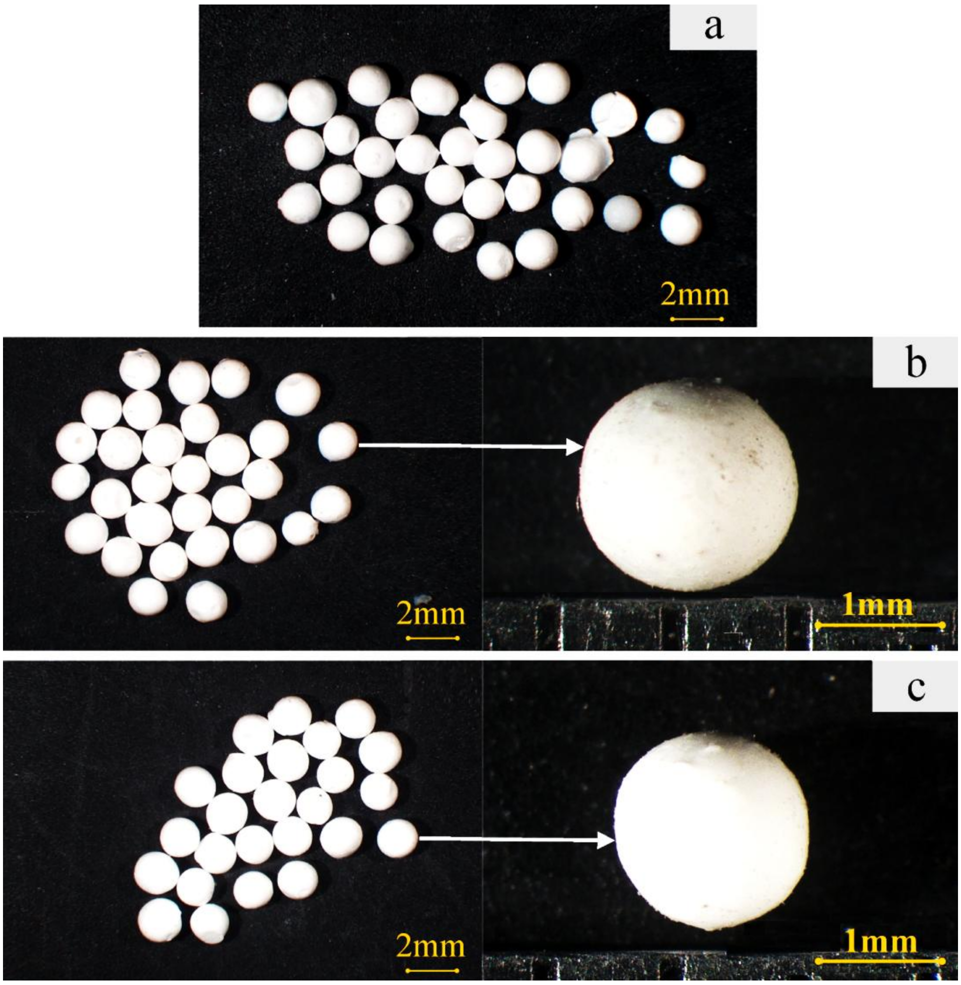

Fig. 3. Optical photograph of (a) 12NS before calcination, (b) 12NS-450, and (c) 12NS-750 granules in two magnifications.

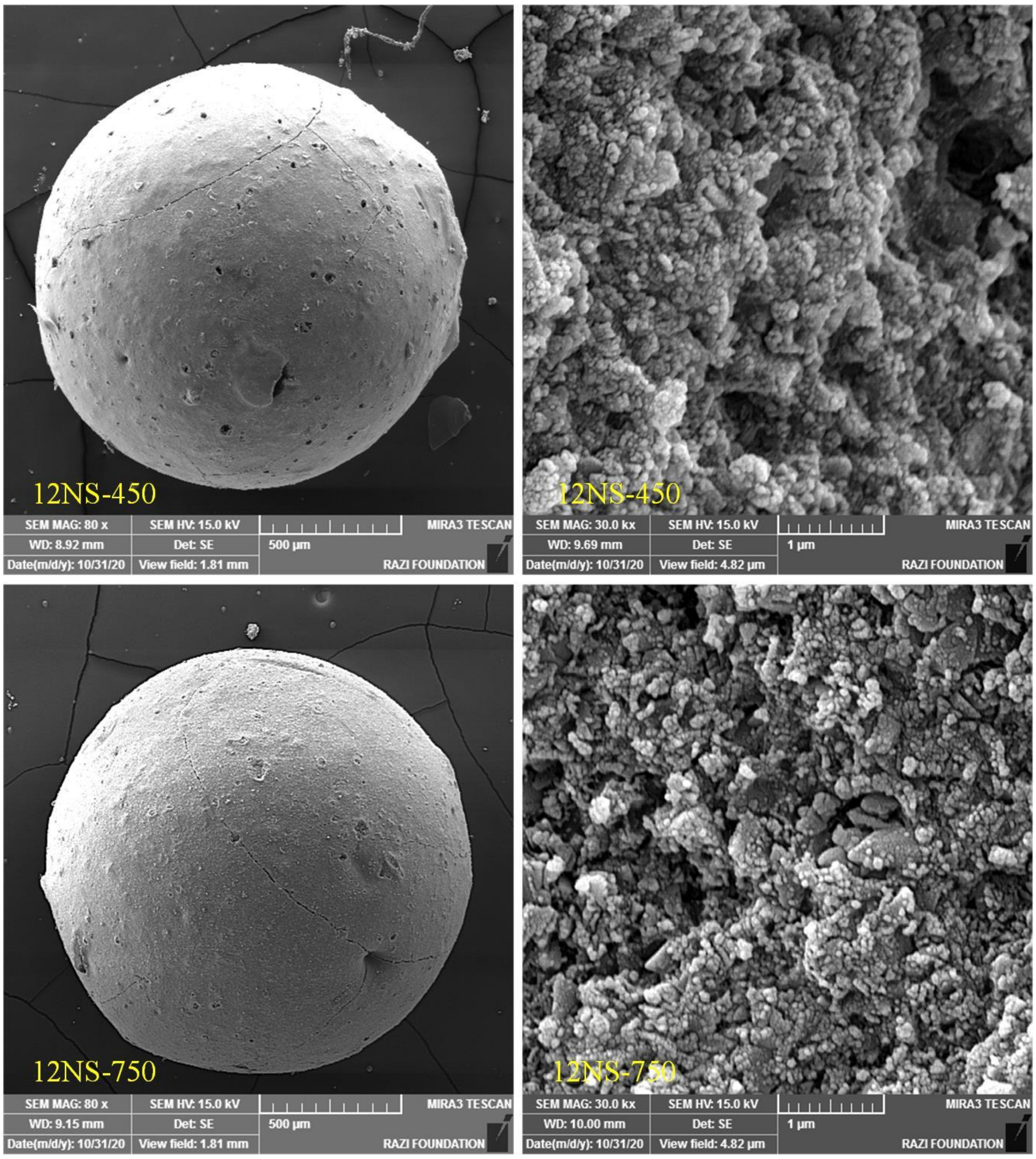

Fig. 4. SEM micrographs of (a) 12NS-450 and (b) 12NS-750.

Table 3. Comparison of BET analysis of 12NS-450 and 12NS-750 granules with other research.

Catalyst	Ref.	BET Analysis			
		Pore Volume (cm^3/g)	Pore Diameter (nm)	BET Surface Area (m^2/g)	pH
12NS–450	This study	0.42	4.94	346.02	-
12NS–750	This study	0.46	8.80	211.41	-
acid-leachates	[36]	0.54	5.8	460	8.0
biopolymer (chitosan)	[37]	0.65	-	464	8.0
aluminum sulfate	[38]	2.3	19.2	412	8.0
polyaluminium chloride solution	[39]	0.59	6.9	339	7.0
alkoxide	[40]	0.89 - 1.58	7-12	293.7 – 387.7	2-3

°C to 580 °C corresponds to the transformation to γ-alumina. Finally, at temperatures up to 850 °C, the sample changes toward the formation of a phase transition peak from gamma-alumina to delta, theta, and alpha-alumina [42]. The phase transition from boehmite to gamma-alumina

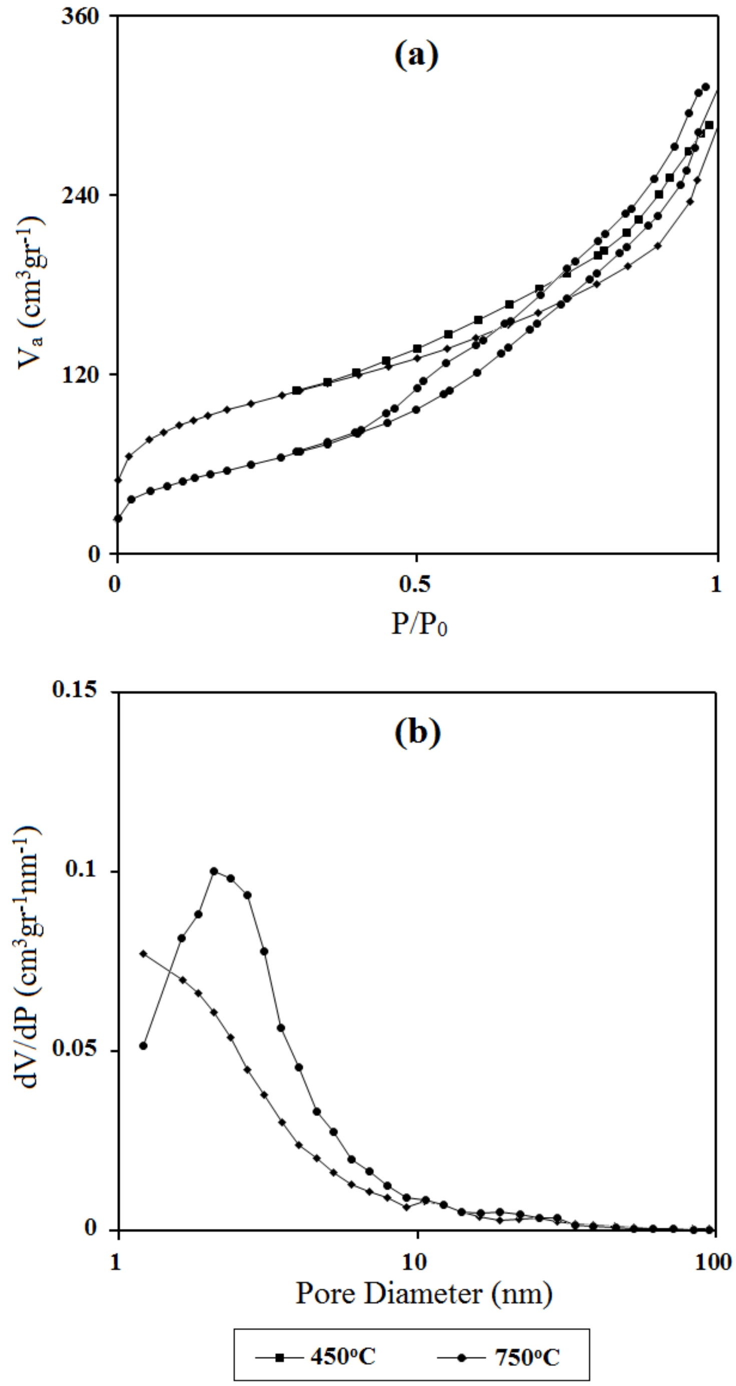

Fig. 5. (a) Nitrogen adsorption–desorption isotherms and (b) pore size distribution curves for the sample 12NS at different calcination temperatures.

begins at about 450 °C and develops with increasing temperature to 750 °C. The main weight loss occurs below 400 °C, and the total mass loss of the sample was 45.23%.

X-ray diffraction analysis

The crystalline structure of alumina granules was studied by wide-angle X-ray diffraction, applying a powder X-ray diffractometer with Cu-

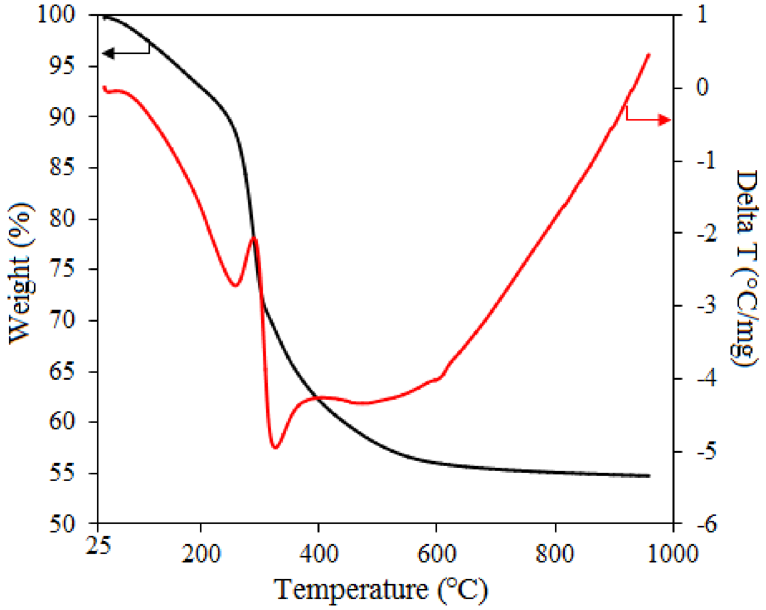

Fig. 6. TGA and DTA curves of the sample 12NS before calcination.

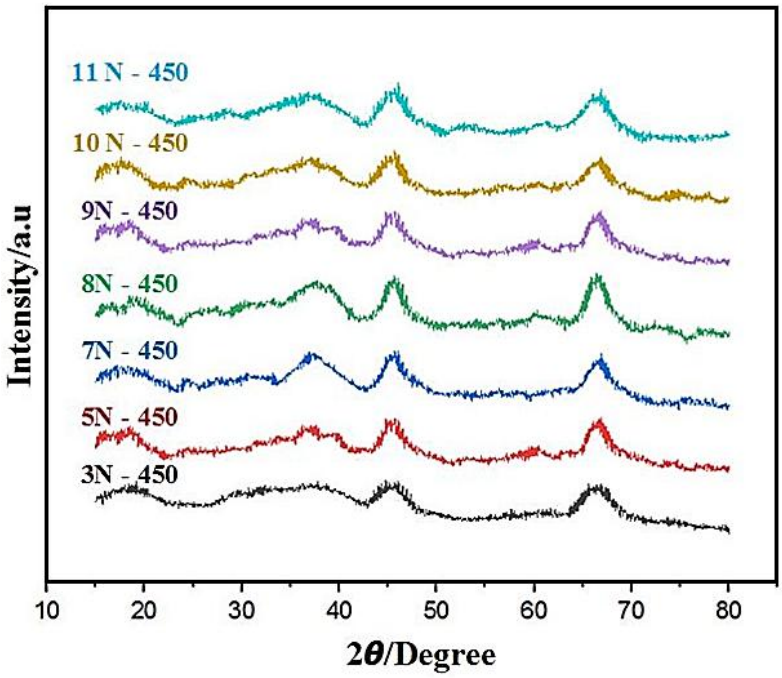

Fig. 7. X-ray diffraction patterns of calcined granules at 450 °C.

Kα source. All scans were noted in the 2θ range of 15–80 ° at a rate of 0.05 per second. Fig. 7 and Fig. 8 shows the X-ray diffraction pattern of alumina granules sintered at 450 ℃ and the optimal samples sintered at 450 ℃ and 750 ℃. The peaks were almost broader exhibit average crystallinity, fine size, and amorphous γ-Al_2O_3 phase. As can be seen, the curve had a standard XRD pattern of γ-alumina at 2θ amounts of 19.56 (111), 31.93 (220), 37.60 (311), 45.79 (400), 66.73 ° (440) (JCPDS File No. 00-029-0063). The X-ray diffraction pattern was correlated with standard data, the 100% intensity happened at a 2θ amount of 66.90 °, which was approximately alike to source data [43]. The γ -alumina sample received in this way shows low crystallinity and there leads to be a peak broadening effect. Initially, boehmite (AlOOH) is formed from the raw material, and then, by increasing the calcination temperature from about 450 °C, boehmite is transferred to the gamma-alumina phase. Finally, about 550 °C, following desorption and dehydration of hydroxyl groups existing on the surface guide to this phase transition is completed of γ-Al_2O_3 which is based on a distorted spinel structure [44,45]. As can be seen from Fig. 8, with increasing the calcination temperature from 450 ℃ to 750 °C, the peaks become thinner and sharper and their

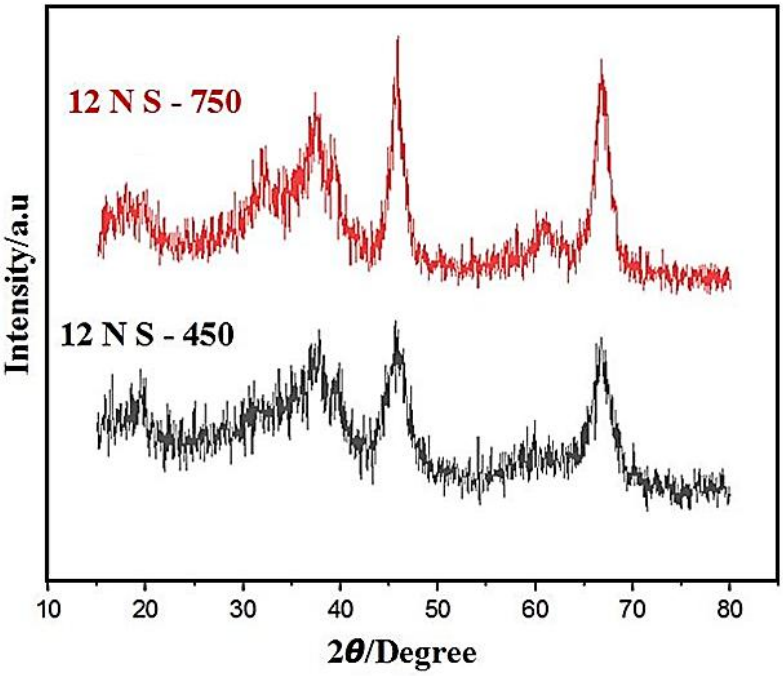

Fig. 8. X-ray diffraction patterns of a sample 12NS calcined at 450 °C and 750 °C.

Table 4. Mechanical strength of calcined γ-alumina granules.

Sample NO.	Mechanical strength (N/Granule)
3 NS-450	25.558
5 NS-450	13.33
7 NS-450	19.838
8 NS-450	17.548
9 NS-450	11.39
10 NS-450	15.97
11 NS-450	13.55
12 NS-450	7.12
12 NS-750	8.52

intensity increases, which is a sign of the growth of gamma-alumina crystals and the evolution of its formation. With boehmite heat treatment, gradually increasing the temperature while the oxygen layers are constant, the hydroxide layers disappear and the body of the gamma-alumina structure is formed. This is logical with the location of the Al^{3+} ions any by the tetrahedral or octahedral positions in the spinel structure.

Mechanical strength

A universal testing instrument was utilized to measure the mechanical strength for granules with higher apparent strength, which was exerted as the maximum pressure applied to break the granule [46]. For each sample, five tests were taken, the average of which was reported in Table 4. The granule calcined at 750 °C gives higher crushing strength, as compared to in the case of calcined at 450 °C. The increase of mechanical strength of the granule could be assigned to the formation of a solid network with highly interconnected particles during the calcination which aids highly compact structure [47]. The gel shrinks under the capillary force during the calcination as the liquid evaporates, enhances the mechanical strength of the granules [48].

Catalytic activity evaluation

The properties of supports caused variation of catalytic properties towards hydrazine monohydrate decomposition. Additionally, it was found that precursor of these supports exerted significant influence on the catalytic properties of the resulting catalyst. As presented in Fig. 9, the optimum support (based on above analyses) for 12NS-450-based catalyst exhibited a rate of 129 h^{-1} and an H_2 selectivity of 22 % without any crushing and mass loss. The amount of releasing hydrogen and nitrogen gases shows that a large amount of N_2 is produced on the iridium surface. This catalyst iridium on Al_2O_3 in laboratory-scale testing shows the larger hydrazine decomposition rate, as shown in other studies [49,50], providing the most efficient decomposition process. It was noted that properly controlling loading percentages can positively and significantly impact the catalytic efficiency. The catalysts without crushing are therefore a promising candidate for hydrazine decomposition in high technology for some purposes in harsh condition because of their strong mechanical strength.

CONCLUSION

The purpose of this work was to study the effect of support on the iridium catalyst for hydrazine monohydrate decomposition. Spherical alumina granules in γ form were successfully prepared from aluminium rich solution extracted from aluminium nitrate using a modified oil-drop method. During

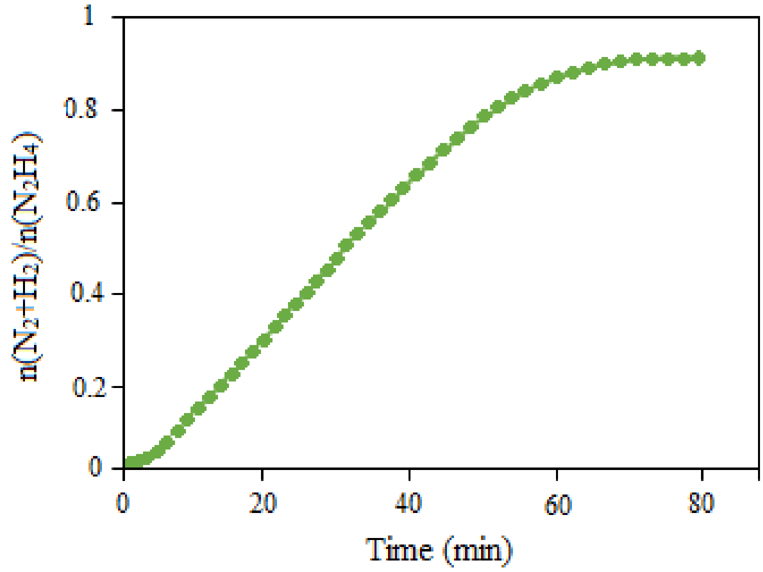

Fig. 9. Hydrazine monohydrate decomposition curve for iridium catalysts prepared with the 12NS-450 support granules.

the preparation of granules, it was found that the concentration of the solution, the ratio of [OH] or [H] to [Al], the calcined temperature, etc. play an important role in controlling the shape, size and stability of the samples. The spherical granule with a mean diameter 1.7 mm was achieved at the molar ratio of [OH] and [H] to [Al] 2.8 and 0.026, respectively, attended by calcination at 450 °C and 750 °C. The granules after calcination had a high surface area (346.02 and 211.41 m^2/g) developed pore volume (0.43 and 0.47 cm^3/gr) and average pore size (4.96 and 8.80 nm). The calcination process at higher temperature adversely affects the porosity and surface area of the prepared alumina granules. The selectivity to hydrogen selectivity and reaction rate of calcined granules in 450 °C for the hydrazine monohydrate decomposition test was 22 % and 129 h^{-1}, respectively. The destruction of supports under high operating temperatures and pressures is one of the major challenges in harsh operations; therefore, our studies are warranted to continue research about the use of these catalysts for hydrazine without grain crushing.

CONFLICT OF INTEREST

The authors declare that there is no conflict of interests regarding the publication of this manuscript.

REFERENCES

1. Jasim Awadh A, Ammar SH, Altabbakh BA. Preparation and characteristics of CuO/γ- Al_2O_3 nanocomposite as efficient adsorbent for adsorption of sulfur compounds from Iraqi naphtha. Materials Today: Proceedings. 2021;42:2596-2602.
2. Sedor KE, Hossain MM, de Lasa HI. Reduction kinetics of a fluidizable nickel–alumina oxygen carrier for chemical-looping combustion. The Canadian Journal of Chemical Engineering. 2008;86(3):323-334.
3. Hossain MM. Chemical-Looping Combustion With Gaseous Fuels: Thermodynamic Parametric Modeling. Arabian Journal for Science and Engineering. 2014;39(5):3415-3421.
4. Akia M, Alavi SM, Rezaei M, Yan Z-F. Synthesis of high surface area γ-Al_2O_3 as an efficient catalyst support for dehydrogenation of n-dodecane. J Porous Mater. 2009;17(1):85-90.
5. Antzara A, Heracleous E, Silvester L, Bukur DB, Lemonidou AA. Activity study of NiO-based oxygen carriers in chemical looping steam methane reforming. Catal Today. 2016;272:32-41.
6. Van Mao RL, Vu NT, Al-Yassir N, François N, Monnier J. The Thermocatalytic Cracking Process for the Production of Light Olefins and Transportation Fuels from Gas Oils. Top Catal. 2006;37(2-4):107-112.
7. Adamu S, Khan MY, Razzak SA, Hossain MM. Ceria-stabilized meso- Al_2O_3: synthesis, characterization and desorption kinetics. J Porous Mater. 2017;24(5):1343-1352.
8. Sánchez-De la Torre F, De la Rosa JR, Kharisov BI, Lucio-Ortiz CJ. Preparation and Characterization of Cu and Ni on Alumina Supports and Their Use in the Synthesis of Low-Temperature Metal-Phthalocyanine Using a Parallel-Plate Reactor. Materials (Basel, Switzerland). 2013;6(10):4324-4344.
9. Moghadam H, Samimi M, Samimi A, Khorram M. Electro-spray of high viscous liquids for producing mono-sized spherical alginate beads. Particuology. 2008;6(4):271-275.
10. Samimi A, Zakeri M, Maleki B, Mohebbi-Kalhori D. Experimental and statistical assessments of the mechanical strength reliability of gamma alumina catalyst supports. Particuology. 2015;21:74-81.
11. Amrousse R, Hori K, Fetimi W. Corrigendum to “Iridium dispersion control in Ir/ Al_2O_3–SiO_2 catalysts by calcination temperature using chloroiridic acid as catalyst precursor” [Catal. Commun. 27 (2012) 174–178]. Catal Commun. 2014;52:57.
12. Soares Neto TG, Dias FF, Cobo AJG, Cruz GM. Evolution of textural properties and performance of Ir/Al_2O_3 catalysts during hydrazine catalytic decomposition in a 2N satellite thruster. Chem Eng J. 2011;173(1):220-225.
13. Amirsardari Z, Vahidshad Y, Amirifar MA, Khodabakhshi AH, Dourani A, Ghadiri Massoom N. Method for Preventing the Contamination of Iridium Nanocatalyst during Plasma Arc Welding Procedure. Journal of Failure Analysis and Prevention. 2021;21(4):1289-1296.
14. Amirsardari Z, Dourani A, Amirifar MA, Massoom NG, Jahannama MR. Controlled attachment of ultrafine iridium nanoparticles on mesoporous aluminosilicate granules with carbon nanotubes and acetyl acetone. Mater Chem Phys. 2020;239:122015.
15. Thongsuriwong K, Amornpitoksuk P, Suwanboon S. Corrigendum to “Structure, morphology, photocatalytic and antibacterial activities of ZnO thin films prepared by sol–gel dip-coating method” [Adv. Powder Technol. 24(1) (2013) 275–280]. Adv Powder Technol. 2016;27(2):796.
16. Atashi H, Mansouri M, Hosseini SH, Khorram M, Mirzaei AA, Karimi M, et al. Intrinsic kinetics of the Fischer-Tropsch synthesis over an impregnated cobalt-potassium catalyst. Korean J Chem Eng. 2011;29(3):304-309.
17. Hu Y, Ding H, Li C. Preparation of hollow alumina nanospheres via surfactant-assisted flame spray pyrolysis. Particuology. 2011;9(5):528-532.
18. Liu H, Sun H, Li J, He X, Zhu Z. pH-dependent formation of AACH fibers with tunable diameters and their in situ transformation to alumina nanocrystals with mesoporous structure. Adv Powder Technol. 2012;23(2):164-169.
19. Mikhaylov VI, Maslennikova TP, Ugolkov VL, Krivoshapkin PV. Hydrothermal synthesis, characterization and sorption properties of Al/Fe oxide–oxyhydroxide composite powders. Adv Powder Technol. 2016;27(2):756-764.
20. Barzegar-Bafrooei H, Ebadzadeh T. Synthesis of nanocomposite powders of γ-alumina-carbon nanotube by sol–gel method. Adv Powder Technol. 2011;22(3):366-369.
21. Wu W, Wan Z, Chen W, Yang H, Zhang D. A facile synthesis strategy for structural property control of mesoporous alumina and its effect on catalysis for biodiesel production. Adv Powder Technol. 2014;25(4):1220-1226.
22. Kozawa T, Naito M. Mechanically induced formation of metastable χ- and κ-Al_2O_3 from boehmite. Adv Powder

Technol. 2016;27(3):935-939.

23. Claude V, Garcia HS, Wolfs C, Lambert SD. Elaboration of an Easy Aqueous Sol-Gel Method for the Synthesis of Micro- and Mesoporous &lt;i&gt;γ&lt;/i&gt;- Al_2O_3 Supports. Advances in Materials Physics and Chemistry. 2017;07(07):294-310.
24. Brunauer S, Emmett PH, Teller E. Adsorption of Gases in Multimolecular Layers. Journal of the American Chemical Society. 1938;60(2):309-319.
25. Choi J, Kim J, Yoo KS, Lee TG. Synthesis of mesoporous TiO_2/γ-Al_2O_3 composite granules with different sol composition and calcination temperature. Powder Technol. 2008;181(1):83-88.
26. Buelna G, Lin YS. Preparation of spherical alumina and copper oxide coated alumina sorbents by improved sol–gel granulation process. Microporous Mesoporous Mater. 2001;42(1):67-76.
27. Ismagilov ZR, Shkrabina RA, Koryabkina NA. New technology for production of spherical alumina supports for fluidized bed combustion. Catal Today. 1999;47(1-4):51-71.
28. Chen J-C, Tang C-T. Preparation and application of granular ZnO/Al_2O_3 catalyst for the removal of hazardous trichloroethylene. J Hazard Mater. 2007;142(1-2):88-96.
29. He L, Huang Y, Liu XY, Li L, Wang A, Wang X, et al. Structural and catalytic properties of supported Ni–Ir alloy catalysts for H_2 generation via hydrous hydrazine decomposition. Applied Catalysis B: Environmental. 2014;147:779-788.
30. Beiknejad D. Synthesis optimization, structural evolution and optical properties of hierarchical nanoporous alumina microspheres prepared by continuous soft chemistry method. J Porous Mater. 2013;20(5):1075-1086.
31. Belekar RM, Dhoble SJ. Activated Alumina Granules with nanoscale porosity for water defluoridation. Nano-Structures and Nano-Objects. 2018;16:322-328.
32. Encyclopedia of Finance (2nd edition). Reference Reviews. 2013;27(7):31-32.
33. Oliveira DM, Andrada AS. Synthesis of ordered mesoporous silica MCM-41 with controlled morphology for potential application in controlled drug delivery systems. Cerâmica. 2019;65(374):170-179.
34. Hu Z, Srinivasan MP. Preparation of high-surface-area activated carbons from coconut shell. Microporous Mesoporous Mater. 1999;27(1):11-18.
35. Islam A, Taufiq-Yap YH, Chu C-M, Chan E-S, Ravindra P. Synthesis and characterization of millimetric gamma alumina spherical particles by oil drop granulation method. J Porous Mater. 2011;19(5):807-817.
36. Liu M, Yang H. Large surface area mesoporous Al_2O_3 from kaolin: Methodology and characterization. Applied Clay Science. 2010;50(4):554-559.
37. Fajardo HV, Martins AO, de Almeida RM, Noda LK, Probst LFD, Carreño NLV, et al. Synthesis of mesoporous Al_2O_3 macrospheres using the biopolymer chitosan as a template: A novel active catalyst system for CO_2 reforming of methane. Mater Lett. 2005;59(29-30):3963-3967.
38. Wang W, Zhang K, Yang Y, Liu H, Qiao Z, Luo H. Synthesis of mesoporous Al_2O_3 with large surface area and large pore diameter by improved precipitation method. Microporous Mesoporous Mater. 2014;193:47-53.
39. Inside Cover Picture. Chin J Chem. 2021;39(5):1034-1034.
40. Yi H, Wan Y, Zhang Y, Wang Y, Fei W, Luo G. Controllable preparation of highly uniform γ-alumina microspheres via the sol–gel route for alkoxide in a coaxial microchannel. J Sol-Gel Sci Technol. 2019;93(2):391-401.
41. Badoga S, Sharma RV, Dalai AK, Adjaye J. Synthesis and characterization of mesoporous aluminas with different pore sizes: Application in NiMo supported catalyst for hydrotreating of heavy gas oil. Applied Catalysis A: General. 2015;489:86-97.
42. Alves AK, Berutti FA, Bergmann CP. The Effects of pH on the Preparation of Alumina by Sol-Gel Process. Particulate Science and Technology. 2005;23(4):351-360.
43. Mishra D, Anand S, Panda RK, Das RP. Statistical optimization of conditions for the hydrothermal precipitation of boehmite. Hydrometallurgy. 2000;58(2):169-174.
44. Li G, Smith RL, Inomata H, Arai K. Synthesis and thermal decomposition of nitrate-free boehmite nanocrystals by supercritical hydrothermal conditions. Mater Lett. 2002;53(3):175-179.
45. Yao N, Xiong G, Zhang Y, He M, Yang W. Preparation of novel uniform mesoporous alumina catalysts by the sol–gel method. Catal Today. 2001;68(1-3):97-109.
46. Buelna G, Lin YS, Liu LX, Litster JD. Structural and Mechanical Properties of Nanostructured Granular Alumina Catalysts. Industrial & Engineering Chemistry Research. 2003;42(3):442-447.
47. Apodaca RL. IBM Donates Large Collection of Patent Chemical Structures to NIH/PubChem. Front Matter; 2011.
48. Rui Z, Chen C, Lu Y, Ji H. Anodic Alumina Supported Pt Catalyst for Total Oxidation of Trace Toluene. Chin J Chem Eng. 2014;22(8):882-887.
49. Amirsardari Z, Dourani A, Amirifar MA, Ghadiri Massoom N, Javadi A, Ehsani R, et al. Dentate number and functionality of O, N-donor ligands for the growth and catalytic reaction of iridium nanoparticles. Chemical Papers. 2020;74(10):3233-3241.
50. Amirsardari Z, Dourani A, Amirifar MA, Ghadiri Massoom N, Ehsani R. Development of novel supported iridium nanocatalysts for special catalytic beds. Journal of Nanostructure in Chemistry. 2019;10(1):47-53.